Yields of Stable and Radioactive Rare-Gas Isotopes Formed by 3- and 29-GeV Proton Bombardment of Cu, Ag, Au, and U†

J. Hudis, T. Kirsten,* R. W. Stoenner, and O. A. Schaeffer
Department of Chemistry, Brookhaven National Laboratory, Upton, New York 11973
and Department of Earth and Space Sciences, State University of New York, Stony Brook, New York 11790
(Received 29 January 1970)

The yields of all rare-gas products, including stable species, with half-lives >10 h, produced in 3- and 29-GeV proton bombardment of Cu, Ag, Au, and U were measured. Mass-spectrometric measurements of Ne^{20}, Ne^{21}, Ar^{38}, Kr^{83}, and Xe^{131} represent total chain yields for these mass numbers. Spallation processes can account for Ne yields from Cu; Ar and Kr from Ag; and Xe from Au. Fission and spallation mechanisms satisfactorily describe the Kr from Au and the Kr and Xe from U. Ne and Ar yields from Au and U do not seem to be formed by spallation and fission processes, but appear to result from the same processes which lead to high yields of even lighter fragments previously observed in high-energy reactions.

I. INTRODUCTION

The study of fission and spallation yields from the high-energy bombardment of medium and heavy elements has been restricted, in general, to the measurement of radioactive products. The general patterns of the yields of such products from different targets at incident energies <6 GeV are reasonably well established, especially for light- to medium-mass targets. For heavy targets and higher energies, the experimental data are less numerous. Yield measurements and recoil experiments, as well as emulsion, solid-state-fragment-detector, and track-detector studies, have all helped to elucidate the processes which take place when high-energy particles interact with complex nuclei. However, there are still uncertainties in the relative importance of various competing mechanisms and in the details of these mechanisms.

One reason for these uncertainties is that unlike the situation in low-energy fission, where most of the primary products are neutron rich, radioactive, and thus easily measured, primary products formed in high-energy reactions tend to have peak yields on or close to the line of β stability, and many important yields remain unmeasured.

The yields of stable species are worth measuring for a number of reasons. First, in most cases stable products represent cumulative yields either of neutron-excess or neutron-deficient species only, and often may help to differentiate between the relative yields of competing mechanisms in one mass region. For example, it is known that low-energy fission leads to neutron-excess products, whereas spallation products are in large part neutron-deficient species. Comparing the cumulative yields of neutron-excess to neutron-deficient species in a narrow mass region can thus yield some idea as to the relative importance of these two mechanisms. Second, in a few cases the yield of a stable isotope is the integrated yield of all products of a given mass. Thus, at least for a few mass numbers, the total yield is obtained without the need of extrapolation and interpolation procedures based on a few independent yields. Finally, when independent yields of stable nuclides can be measured they add much needed information to charge-dispersion studies, since the peak yields of these distributions sometimes lie near stability.

Although stable isotopes may be measured by mass spectrometry, this technique has not been widely used in the study of high-energy nuclear reactions. Klapisch[1] has reviewed work in this field completed by 1968, including new developments from the on-line mass-spectrometric procedures developed by Bernas and co-workers.[2] One difficulty is that, in general, mass-spectrometric techniques are not as sensitive as the measurement of radioactivity. However, the mass spectrometry of rare gases has been developed into a very sensitive technique, and it is now possible to measure as few as 10^9–10^{11} atoms of each species.[3]

Since mass spectrometry can also be applied to radioactive species having half-lives exceeding a few hours, the opportunity for yield measurements by two completely independent methods arises. In this way, one may check the absolute calibration of the spectrometer for the different rare gases in each experiment. Thus, in this work, the yields of rare-gas isotopes, stable and radioactive (with $t_{1/2}>10$ h), formed by the bombardment of Cu, Ag, Au, and U with 3- and 29-GeV protons were measured. Because there are no radioactive isotopes of Ne with half-lives long enough to perform the cross calibrations between mass-spectrometric and radioactivity measurements, Na^{22} was measured in each run. Although not a direct calibra-

tion, the regularities of the ratio of Ne^{22} to Na^{22} and of $Ne^{20}:Ne^{21}:(Ne^{22}+Na^{22})$ observed in each experiment gave added confidence to the absolute calibration of the spectrometer for the detection of Ne isotopes.

II. EXPERIMENTAL PROCEDURES

A. Irradiations

Targets generally consisted of a stack of three 0.001-in. aluminum foils to monitor the proton beam, followed by three foils of the target element. Each target foil was 0.002–0.003 in. thick. Target stacks were mounted on frames which were then attached to the electromechanical flip mechanism used at the BNL alternating gradient synchrotron. Irradiations were made at energies of 3 and 29 GeV. Irradiation times varied from 30 to 130 min corresponding to total proton fluxes of between 10^{15} and 10^{17} protons. At least two independent irradiations were performed for each target element at each energy.

The total proton flux through the target assembly was determined from the monitor reaction $Al^{27}(p, 3p3n)Na^{22}$. The monitor cross sections at 3 and 29 GeV were taken as 11[4] and 9.8 mb,[5] respectively. The middle Al foil was used as the proton monitor.

After irradiation, semicircles with the leading edge as the diameter were punched from the target assembly with a $\frac{3}{4}$-in. circular punch. The sensitivity of the mass-spectrometric measurements did not permit discarding the leading edge, so all target assemblies were carefully trimmed before irradiation to minimize the effects of any misalignment of the foils. The foils were then weighed, and the middle target foil was taken for measurement of Na^{22}, Ar^{37}, Ar^{39}, Ar^{42}, Kr^{85}, and Xe^{127} activities, and the inner and outer target foils were used for mass-spectrometric determinations of rare-gas isotopes. One was measured as soon as possible (fresh target); the other one was measured anywhere from a few days to a few months after irradiation (old target).

B. Activity Measurements

The dissolution of the middle target foil and subsequent isolation and purification of the rare-gas radioactivities was carried out in the apparatus shown in Fig. 1. The target foil was introduced into the dissolver vessel (a), after which the air was evacuated from the dissolver section [(a) through (f)], and replaced with helium. Copper and silver foils were dissolved in 6 *N* HNO_3; gold was dissolved in dilute aqua regia; uranium was dissolved in 6 *N* HCl to which had been added a trace of platinic chloride as a catalyst. In each case, 20 mg of Na carrier was added to the acid. During the dissolution, the flow of helium sweep gas was kept very low. After the target was in solution a measured volume of mixed Ar, Kr, Xe carrier was added from pipette (d) and flushed through with helium at the rate of 200 standard cm^3 (s.c.c.) per min for ten minutes. It is estimated that this corresponds to several system volumes. Recovery of added carrier rare gases was quantitative in nearly every experiment.

The effluent gas stream from the dissolving vessel was passed through a purification section (f) consisting sequentially of sodium hydroxide pellets, magnesium perchlorate, hot titanium sponge, hot cupric oxide, soda lime, and finally magnesium perchlorate. The dried purified gas then passed through the chromatographic column (g) 6 mm i.d. $\times$280 mm, filled with activated charcoal, and immersed in liquid nitrogen. After the initial ten-

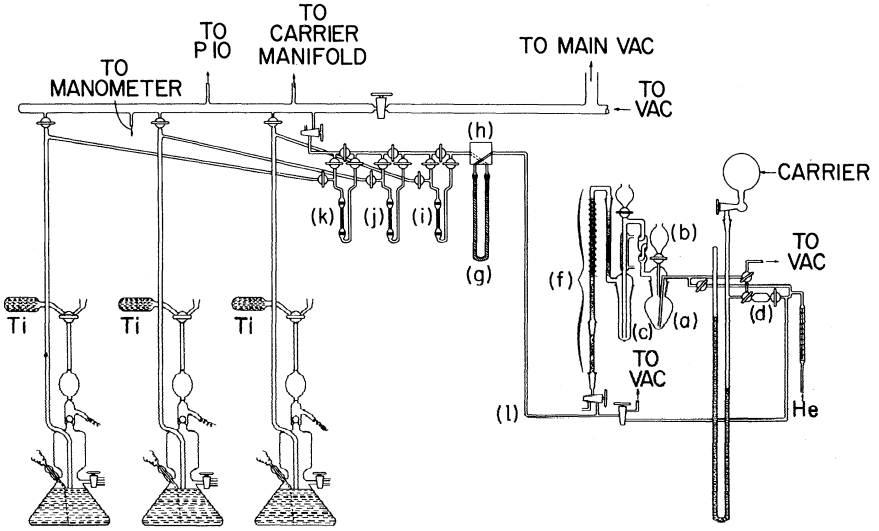

FIG. 1. Apparatus for separation and purification of rare gases. Components identified with lower case letters are described in the text.

minute sweep period was completed, appropriate stopcocks were turned to permit the helium to bypass the dissolving vessel, and the flow rate of helium was reduced to 70 s.c.c. per min before eluting the rare gases from the chromatographic column.

The elution of the individual rare gases was observed by means of the thermal-conductivity cell (h). The elution of the rare gases was commenced by replacing the liquid nitrogen bath on the chromatographic column (g) with an acetone bath at -25° C. At this temperature, argon was eluted very rapidly, and krypton began to emerge after approximately ten minutes, at which point the acetone bath at -25°C was replaced by a water bath at +50°C. This temperature caused krypton to be eluted very quickly, and xenon appeared after about 15 minutes. The elution of xenon was completed by replacing the water bath with a heating mantle at 360°C. Argon, krypton, and xenon were collected, respectively, on small charcoal traps (i), (j), and (k) immersed in liquid nitrogen, by diverting the gas stream through each trap at the appropriate time as determined by the signal from the thermal-conductivity cell. With the traps still immersed in liquid nitrogen, the helium was pumped away to vacuum, after which the traps were heated to 200° C. with heating mantles, and the individual rare gases were transferred by means of the Toepler pumps to hot titanium furnaces located at the top of each pump.

Ar^{37} activity was measured by taking a small aliquot of the argon fraction into a gas proportional counter (1.3 cm i.d. × 30 cm) filled with P-10 (10% methane-90% argon) to 1 atm. A small correction was made to the counting rate for the contribution of Ar^{39}, Ar^{42}, and K^{42} activities.

Ar^{39} and Ar^{42} were determined by transferring the remainder of the argon fraction into the envelope surrounding a thin wall detector which was made entirely from quartz to minimize background counting rates. The low-level shield surrounding the counter was sequentially one in. of mercury, a ring of anticoincidence counters, and six in. of iron. After the daughter K^{42} had been allowed to grow to equilibrium, the gross counting rate resulting from contributions of Ar^{39}, Ar^{42}, and K^{42} was measured. The gas sample was removed from the counter, and the K^{42} activity remaining in the counter was then measured. The counting rate of the K^{42} after adjustment to the time of removal of gas from the counter was subtracted from the gross counting rate to yield the counting rate of Ar^{39} and Ar^{42} combined. The counting rate of K^{42} after correction for counting efficiency is the disintegration rate of Ar^{42}. The detection efficiencies of these counters was measured as described before.[6] The Ar^{37} detection efficiency of these counters was less than 3×10^{-5}% as measured using Ar^{37} prepared by the reaction $Ca^{40}(n,\alpha)Ar^{37}$.

Kr^{85} and Xe^{127} activities were measured using gas proportional counters filled with P-10 to 1 atm. Xenon extracted from uranium targets contained 8-day Xe^{129m}, 12-day Xe^{131m}, and 5.27-day Xe^{133}, as well as Xe^{127} which was being sought, so that it was necessary to measure the activity of the xenon fraction for two to three months to resolve the 36.4-day Xe^{127} component. The counting data were analyzed by a least-squares procedure[7] to obtain the counting rate of Xe^{127}.

After the rare gases had been removed from the target solution in the dissolver vessel [(a) in Fig. 1] standard chemical procedures[8] were used to separate and purify the sodium. The purified sodium fraction was mounted as NaCl, and the intensity of the 1.28-MeV γ ray of Na^{22} was determined with a calibrated 3-in. × 3-in NaI detector.

C. Mass-Spectrometric Measurements

Figure 2 shows a sketch of the apparatus used. Both the vacuum line, made of Dow Corning 1720 glass tubing, and the mass spectrometer were baked at 220°C for 10 h before operation. The 1720 glass has a very low diffusion rate for helium, and a static pressure of 10^{-8} Torr was achieved routinely. The mass spectrometer was a statically operated, 60° Nier-type spectrometer. It was equipped with an electron impact ion source and a Cu-Be photomultiplier detector. The output of the photomultiplier was measured with a high-resistance vibrating-reed electrometer.

Blank runs were performed before each measurement. In general, for nuclides formed with cross sections $\geq$1 mb, blank peak heights were $\leq$10% of the sample peak heights except for Ne^{20} and Ar^{36}. In the latter cases, the resulting uncertainties depended on the total number of protons striking the target, and these uncertainties were included in the error limits assigned to the results. No serious problem was encountered with the mass-spectrometer memory effect[3] in the Kr and Xe regions.

To start the separation, the sample was dropped into a molybdenum crucible and melted at 1900°C by induction heating. Maintaining this temperature for 10 minutes liberated all gaseous products from the target. Next, all reactive gases were removed in a furnace containing titanium sponge at 900°C. Both Kr and Xe were collected in a trap at -196°, and Ar was adsorbed onto charcoal at -196°C. The valve between the mass spectrometer and purification line was then opened, and the amounts of Ne^{20}, Ne^{21}, and Ne^{22} present were measured. After pumping away the Ne fraction, the heavier rare gases were successively released from their cold traps

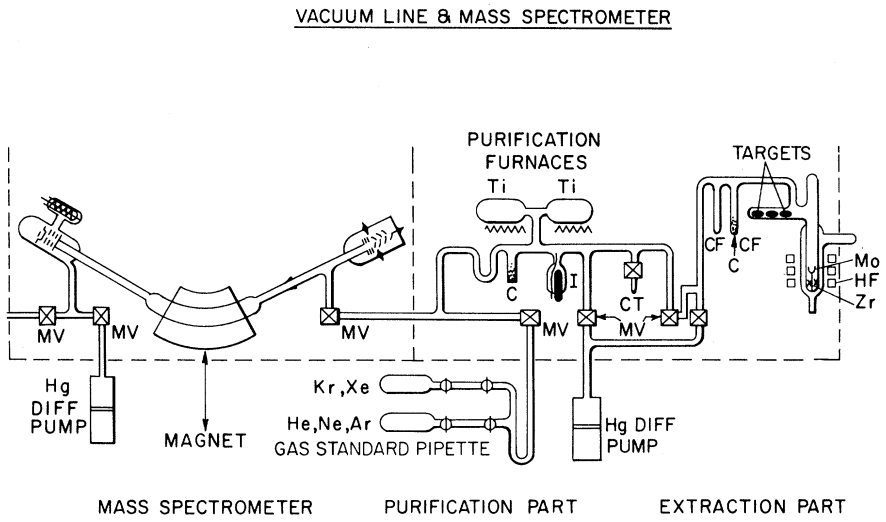

FIG. 2. Mass spectrometer and associated apparatus for the melting of targets, and separation, purification, and analysis of rare gases. HF – high frequency coil; Ti – titanium getter; Mo – molybdenum crucible; CT – cold trap; I – ionization gauge; and C – charcoal.

into the system and measured.

All heavy noble gases (Ar, Kr, and Xe) were collected in a liquid-nitrogen-cooled charcoal trap after measurement and transferred to the vacuum line shown in Fig. 1 where they were diluted with known amounts of inert carrier gas, separated, and purified, after which the radioactivity measurements were made as described before. From U and Au targets it was usually possible to make five independent measurements of five isotopes in each run: Ar^{37}, Ar^{39}, Ar^{42}, Kr^{85}, and Xe^{127} were measured once from the dissolved foil by counting, and both by mass spectrometry and by counting from each of the two remaining foils.

After all of the noble gases had been measured, the target was remelted and the crucible raised to a temperature 100°C higher than originally, and the mass analysis was repeated to make certain that the target was completely outgassed in the main run. Normally, less than 3% of the total yield was found in the second sample, and in the worst case 30% was found. In all cases the measured yields were corrected for this effect. Since many targets were melted in the same crucible, it was essential to outgas the crucible just before each new run. Otherwise noble-gas products could accumulate from the decay of nongaseous parent activities in the melt of the old targets.

The absolute calibration of the mass spectrometer was made by the introduction of precisely known amounts of standard gas samples into the system. Details of the construction and use of the calibration system are described elsewhere.[3] The vacuum system was constructed to allow the measurement of freshly irradiated targets within a short time. The target was introduced into the vacuum system by means of a vacuum lock, shown in Fig. 3. Under favorable conditions, it was possible to measure rare gases 12 h after the end of the irradiation.

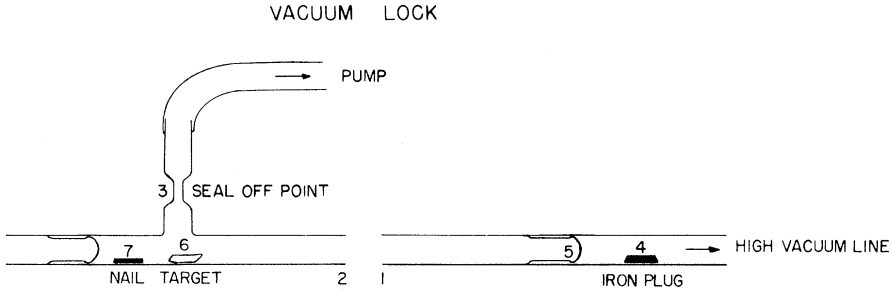

FIG. 3. Vacuum lock for introduction of target foils to mass-spectrometer vacuum system. The procedure followed was: connect (1) and (2); pump out lock with fore pump and seal at (3); break glass seal (5) with iron plug (4); pump with diffusion pump; then using nail (7) push target (6) into furnace (not shown).

TABLE I. Cumulative yields, in mb, for rare-gas isotopes formed by 3- and 29-GeV proton bombardment of Cu, Ag, Au, and U. T designates total isobaric yield.

	Cu				Ag				Au				U			
	Expt.		Calc.		Expt.		Calc.		Expt.		Calc.		Expt.		Calc.	
	3	29	3	29	3	29	3	29	3	29	3	29	3	29	3	29
Ne 20	7.4± 0.6	8.5± 1	5.4	7.6	6.5± 0.8	15 ± 1.5			10.7± 1	26.0± 0.8			10 ± 2	38 ± 3		
21 T	7.4± 0.4	8.7± 0.8	5.7	7.9	6.5± 0.6	15 ± 1.5			10.3± 1	26.0± 0.8			9.9± 1	38 ± 3		
22	7.2± 0.5	8.1± 0.9	6.0	8.1	6.1± 0.6	13.7± 1.8			12.5± 1.2	24.0± 1			10 ± 1	36.9± 3		
Ar 36	1.4 ± 0.1	1.2 ± 0.1	1.0	1.0	0.31± 0.05	0.47± 0.05	0.3	0.6	~0.1	0.28± 0.03			<0.5	0.20± 0.05		
37	5.4 ± 0.4	4.7 ± 0.4	5.7	5.9	1.2 ± 0.15	2.3 ± 0.3	1.7	3.2	0.52± 0.1	1.6 ± 0.1			0.40± 0.1	1.6 ± 0.3		
38 T	13.4 ± 0.7	11.1 ± 1	13.3	13.4	4.4 ± 0.4	7.0 ± 0.5	3.9	7.1	4.7 ± 0.5	9.4 ± 0.6			11.2 ± 2.5	15.3 ± 1		
39	7.2 ± 0.4	6.4 ± 0.5	9.0	9.0	2.7 ± 0.3	4.7 ± 0.4	2.6	4.7	3.5 ± 0.5	7.8 ± 0.4			7.0 ± 1.5	13 ± 1		
42	0.17± 0.02	0.16± 0.03	0.1	0.1	0.12± 0.02	0.21± 0.03	0	0.05	0.42± 0.06	0.82± 0.05			1.2 ± 0.1	2.0 ± 0.3		
Kr 76					2.0 ± 0.2	1.4 ± 0.3	1.2	1.0	···	···	0.2	0.5	···	···	0.1	0.3
78					11.1 ± 1	8.9 ± 0.8	9.8	8.0	1.58± 0.1	2.8 ± 0.4	1.7	3.5	1.0± 0.3	2.7± 0.3	0.6	2.1
79					12.7 ± 1.5	11.4 ± 1	14.9	11.9	···	4.2 ± 0.3	2.6	5.2	<4	5.3± 0.5	1.0	3.1
80					16.6 ± 1.5	13.2 ± 1	17.9	14.0	4.8 ± 0.4	6.8 ± 0.5	3.0	6.1	13.6± 1	13.7± 1.5	1.2	3.6
81					17.0 ± 1.5	13.6 ± 1	18.3	14.1	4.4 ± 0.4	6.4 ± 0.4	3.1	6.1	9.8± 1	10.7± 1	1.2	3.6
82					17.7 ± 1.5	14.1 ± 1	19.2	14.5	5.4 ± 0.5	7.1 ± 0.5	3.2	6.2	19.5± 2	19.6± 2	1.2	3.6
83 T					17.9 ± 1.5	14.3 ± 1	19.9	14.7	5.9 ± 0.6	7.3 ± 0.5	3.3	6.3	30 ± 3	28.3± 2	1.2	3.7
84					1.8 ± 0.3	1.55 ± 0.2	2.2	1.6	2.4 ± 0.3	2.7 ± 0.4	0.4	0.7	26 ± 5	23 ± 2	0.1	0.4
85					0.03± 0.01	0.023± 0.004	0.02	0.02	0.34± 0.04	0.26± 0.02	0	0.01	8 ± 1	7.7± 0.8	0	0.01
86					<0.02	<0.02	0	0	0.23± 0.05	~0.1	0	0	12 ± 1	13.1± 1	0	0
Xe 122									···	7.6 ± 0.5	4.8	5.7	<1	4.9± 0.5	1.6	3.1
124									8.4 ± 0.6	7.9 ± 0.4	7.8	8.8	4.5± 0.5	6.6± 1	2.6	4.9
125									···	7.7 ± 0.5	8.4	9.4	6.0± 0.8	6.4± 1	2.8	5.2
126									9.2 ± 0.6	8.2 ± 0.5	8.7	9.7	8.2± 1	10 ± 1	2.9	5.3
127									9.6 ± 0.6	7.9 ± 0.5	9.0	9.9	7.5± 1	9.4± 1	2.9	5.4
128									9.6 ± 0.6	8.0 ± 0.5	9.2	10.0	9.3± 1	12.9± 1	3.0	5.5
129									9.9 ± 0.6	8.2 ± 0.5	9.4	10.1	8.8± 1	10.4± 1	3.1	5.5
130									0.15± 0.04	~0.1	0.3	0.3	8.1± 1	8.2± 1	0.1	0.2
131 T									9.9 ± 0.6	8.2 ± 0.5	9.9	10.3	16 ± 2	23.5± 2	3.2	5.6
132									<0.03	<0.01	0	0	13.1± 1	16 ± 2	0	0
133									···	···	0	0	~13	26 ± 6	0	0
134									<0.03	<0.01	0	0	10.7± 1	14.5± 2	0	0
135									···	···	0	0	~15	···	0	0
136									<0.03	<0.01	0	0	8.4± 0.8	12.1± 2	0	0

III. RESULTS

The experimentally measured cross sections are shown in Table I. The cross sections listed represent cumulative yields including all precursors with half-lives <3 yr. At least two irradiations were made for each target-energy combination. In addition, some Ag targets from earlier irradiations were also available.[9] Results obtained on these old targets were included in the computation of the final results. This helped to increase the precision of some yield determinations, especially for those rare-gas isotopes which have relatively long-lived precursors, e.g., Rb^{83} ($t_{1/2}=83$ day), Rb^{84} ($t_{1/2}=33$ day), and Sr^{82} ($t_{1/2}=25$ day).

The errors shown in Table I were estimated from the internal consistency of the data. The following points were considered:
(a) agreement between radioactivity measurements made on the dissolved foil with the radioactivity measurements made on the gas samples collected from the spectrometer after the analysis of the other two foils from the same run,
(b) agreement between mass-spectrometric results from the two foils in each experiment for those rare-gas nuclides fed by precursers with half-lives < a few hours,
(c) agreement between radioactivity and mass-spectrometry results for Ar^{37}, Ar^{39}, Ar^{42}, Kr^{85}, and Xe^{127} within one run,
(d) agreement between results of duplicate experiments.

In general, the spread in measured cross-section values for each product was no greater than ±15%. This observation serves, in item (c) above, as a check on the relative detection efficiencies of the counters and of the mass spectrometer.

There were, in a few cases, some rather large discrepancies. These discrepancies were not systematic; they occurred usually in only one of the four tests listed above, and were not included when the average values listed in Table I were calculated. Occasionally, the reason for the discrepancies was obvious; incomplete outgassing and incomplete collection of the products in the spectrometer or misalignment of the three target foils.

There are two possible sources of error arising from Ne recoils. The target foil next to the Al monitor foils may collect Ne recoils from the monitor. It has been shown previously that <1% of the Na^{24} produced in GeV reactions recoils out of 0.003-in Al foil.[10] Assuming that $\sigma_{Al\rightarrow Ne}\approx 20$ mb, and that all the recoiling Ne atoms are trapped in the first target foil, there is, at most, a 3% effect, and no corrections were made.

A second source of error is the recoil loss of Ne from the target foils. One can show, using mean recoil ranges of Na^{24} as determined by Crespo, Alexander, and Hyde[11] that corrections for the Cu, Ag, and U targets are <5%. For Au targets (three 0.002-in. foils), there is a 10% loss of Ne in the upstream foil due to uncompensated forward recoils and a 5% loss in the downstream foil due to uncompensated backward recoils. The Ne results for Au in Table I, which were obtained by averaging data from the upstream and downstream foils, were increased by 7% to correct for recoil loss.

The poorest set of data are the yields from U plus 3-GeV protons. The integrated proton fluxes obtained in these irradiations were the lowest of all the experiments, and thus the amounts of product atoms were small. In neither 3-GeV proton + U irradiation was it possible to detect Na^{22} from the dissolved foil, and the total Ne^{22} and Na^{22} figure in Table I was obtained from the mass-spectrometric measurements and the Na^{22} cross section previously reported.[12]

In one U + 3-GeV proton experiment, incomplete outgassing was obvious from the results, although not from the specific outgassing check described previously. With this experiment, the absolute amounts of radioactive Ar, Kr, and Xe products were obtained from the counting measurements, and the isotopic ratios determined by mass spectrometry were then used to determine the yields of the stable and long-lived species. The same method could not be used to determine the Ne yields, since there was no radioactive isotope of Ne measured. Here the extraction efficiency was calculated from the Ar results and presumed to apply to the Ne yields.

Although the U + 3-GeV proton data are somewhat in doubt, they have been included in Table I because the error of ratios of stable isotopes within one rare gas is at least three times smaller than the absolute errors.

As described previously, two foils from each target stack were measured on the mass spectrometer, one hours, and the second, anywhere from days to months after the irradiation. Thus it was possible to obtain independent yields of a few nu-

TABLE II. Independent yields, in mb, at 29 GeV.

Au		U	
Br^{82}		3.8 ±25%	3.7[a]
Rb^{84}	1.7 ±25%	8.0 ±25%	5.2,[b] 4.0[a]
I^{126}	<0.2	3.4 ±25%	3.0[c]
Xe^{129}	<0.3	3.2 ±25%	3.0[c]
Xe^{131}	<0.1	2.5 ±25%	2.5[c]

[a] J. Chaumont, private communication.
[b] Ref. 29 (6.2 GeV).
[c] Interpolated values from N/Z versus yield curve in the mass-130 region from Ref. 14.

clides at 29 GeV (Table II). The errors associated with these yields are estimated to be ±25%. No results are given for 3-GeV irradiations because, as mentioned above, the U+3-GeV proton cross sections are suspect.

IV. DISCUSSION

A number of the yields reported here, Ne^{20}, Ne^{21}, Ar^{38}, Kr^{83}, Xe^{131}, represent the total yield for those mass chains. These points are especially valuable in defining the mass-yield curves for the targets and energies used in this work, because the usual interpolation techniques used to obtain total isobaric yields from a few measured independent yields are unnecessary.

Many of the data in Table I already have been used to obtain the mass-yield curves for Ag,[13] Pb-Au,[14] and U[14] at 3 and 29 GeV. Figures 4 and 5 show the mass-yield curves from Au and U at 29 GeV. In Fig. 4 the point $A=7$ is from R. Klapish.[15] For both targets it is obvious that yields in the mass-40 region and below are formed to a large extent by mechanisms other than spallation or fission. From Ag,[13] products in the mass-40 region seem to be the tail of the spallation yield distribution, and it will be shown that calculations agree with this premise. The most obvious difference between the Au and U curves is the large fission contribution to the measured U yields and the absence of a discernable fission-product peak in the Au mass-yield curve. Fission cross-section measurements using mica detectors[16] showed that $\sigma_f(\mathrm{U})=670$ mb and $\sigma_f(\mathrm{Au})=63$ mb at 29 GeV. Thus, although fission is the major contribution to yields

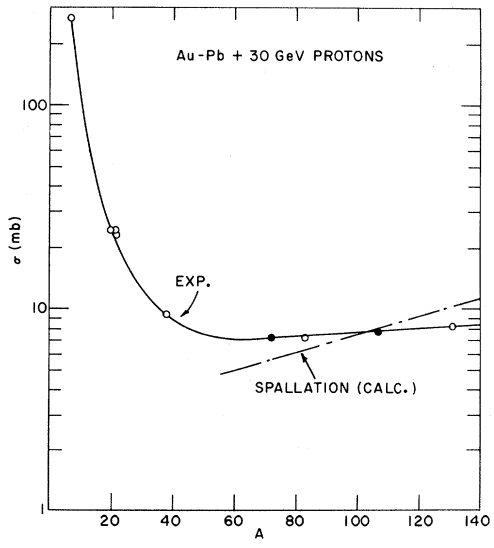

FIG. 4. Mass-yield distribution from Au+29-GeV protons.

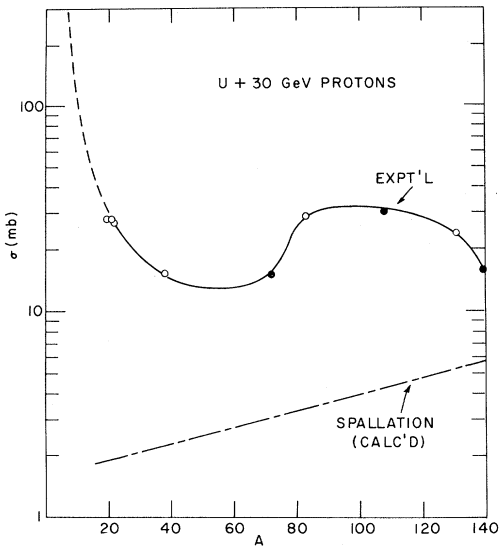

FIG. 5. Mass-yield distribution from U+30-GeV protons. The dashed section is an extrapolation based on the Au results in Fig. 4.

in the mass region 70–150 from U, the Au results in this mass region can be explained by spallation processes corrected for a small amount of fission.

Rudstam[17] has developed a semiempirical formula which has been quite successful in correlating the spallation yields of a wide variety of products, especially from targets in the region Cu–Ag. In this formula, the yield of spallation products is assumed to decrease exponentially with increasing mass difference between target and products, and the distribution of isobaric yields in a mass chain is assumed to be either Gaussian or approximately so. Schwarz and Oeschger[18] have approximated the Rudstam equation with an integral and obtained:

$$\sigma(\Delta A, E_0, A_t) = \sigma_0 A_t^{2/3} p e^{-p\Delta A}, \tag{1}$$

where ΔA is the mass difference between target and product, E_0 is the incident energy, A_t is the target mass, and σ_0 is a constant. Schwarz and Oeschger also give an interpolation formula for p as a function of E_0 and A_t for Al, Cu, and Ru at energies between 0.1 and 2 GeV:

$$p \approx C_1 E_0^{-2/3} \frac{1}{1+C_2 A_t}, \tag{2}$$

where $C_1=0.237$ GeV$^{2/3}$ and $C_2=0.020$. These relationships plus the charge distribution of Rudstam[16]:

$$\exp\left(-11.8 A_p^{-0.45} \left| Z_p - 0.486 A_p + 0.00038 A_p^{2} \right|^{3/2}\right), \tag{3}$$

where A_p and Z_p are the mass and charge of the product, were used to calculate the spallation cross sections shown in Table I.

The constant σ_0 in Eq. (1) is ~60 for Cu at 5.7 GeV, and since little is known about the energy and target dependence of this figure the same value was used for all targets at both 3 and 29 GeV. Rudstam has shown that the parameter p decreases with increasing energy up to 6–10 GeV and then remains constant; the lighter the target the lower the energy at which p becomes energy independent. For Cu the critical energy is ~6 GeV, and for Ag, Au, and U the critical energy is not well determined but is known to be 10 GeV or less. To compare calculations with the 29-GeV Cu results, p was calculated from Eq. (2) at 6 GeV, and the results are listed in Table I. For Ag, Au, and U calculations, 10 GeV was taken as the energy at which p becomes energy independent to use in Eq. (1).

From Au and U, the fission cross sections[16] measured at 3 and 29 GeV were subtracted from the $\sigma_0 A^{2/3}$ term to eliminate that part of the total cross section not available for spallation.

The agreement between calculated and experimental results is quite good. Both the total yields of Ne isotopes, and the total yield and isotopic distribution of Ar isotopes from Cu (Fig. 6) and of Ar and Kr species from Ag (Fig. 7), are reproduced satisfactorily by the calculation. The calculation is in good agreement with Xe yields from Au, but predicts lower yields for Kr than were measured. This too is reasonable when one remembers that the 63-mb fission cross section of Au will produce 126 mb of yield, most of it in the mass region 70–100. From U, where fission is

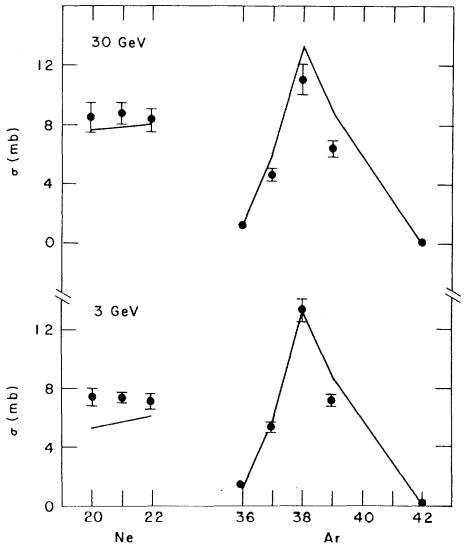

FIG. 6. Yield distribution of Ne and Ar isotopes formed in the bombardment of Cu with 29-GeV protons. The points are experimental, the lines connect calculated spallation yields (not shown) from Table I.

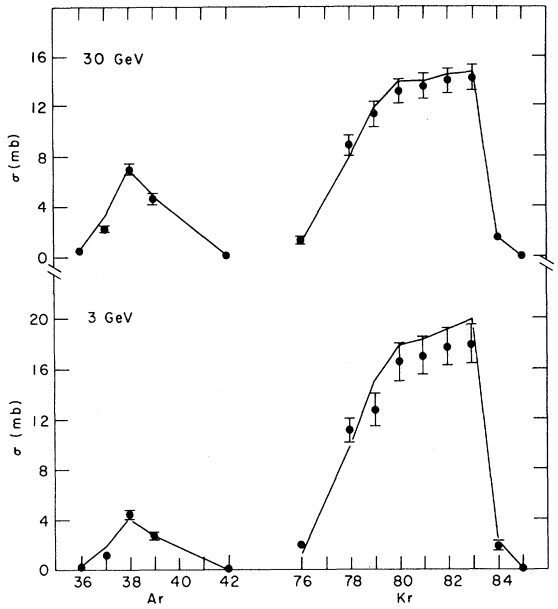

FIG. 7. Yield distribution of Ar and Kr isotopes formed in the bombardment of Ag with 29-GeV protons. The points are experimental, the lines connect calculated spallation yields (not shown) from Table I.

an important contributor in both the Kr and Xe mass region, the calculated results give at least a rough idea of the spallation contribution, as shown in Fig. 5.

Ne^{20-22} *and* Na^{22}. The process or processes by which fragments with masses between 18 and 30 are produced in the interaction of GeV protons with complex nuclei has been a puzzle ever since they were first observed. The results reported here provide a systematic study of the total yields at three mass numbers, 20, 21, and 22, as a function of target mass at two energies. In addition, the data yield the ratio of the cumulative neutron-deficient yield to the total yield at $A = 22$.

The spallation process is a mechanism which has been successful in predicting the wide variety of final products observed in high-energy nuclear reactions at incident energies >100 MeV. Spallation products are the residual nuclei left after a larger or smaller number of nucleons and small nuclei (e.g. He^3, He^4) have been emitted from the struck target during the fast nucleonic cascade and the slower evaporation stage of deexcitation. Both the nucleonic cascade[19,20] and the evaporation process[21,22] have been the subject of calculations, the results of which are in reasonable agreement with observations. At the present time no such detailed calculations are availabel for incident energies >2 GeV.

As mentioned previously, the calculated spallation cross sections of mass-20–22 products from

Cu (Table I) agree, especially at 29 GeV, with experiment. However, the calculations predict a 10% lower cumulative yield for Ne^{20} than for Ne^{22} at both 3 and 29 GeV, which is not observed experimentally. Within experimental error, measurements on all targets, at both energies, yield $\sigma(A = 20) = \sigma(A = 21) = \sigma(A = 22)$. Thus, the data show that spallation can account for most of the observed mass-20–22 products from Cu at 3 and 29 GeV. They also suggest that another mechanism, one in which yield increases with increasing mass of fragments, may contribute to the yield of fragments even from light targets.

There is only a small change (10–15%) in the Ne yields from Cu between 3 and 29 GeV. Similar small changes have been reported previously for a wide varirty of products from Cu between these two energies.[23] The Ne yields from Ag, Au, and U targets increase by factors of 2, 3, and 4, respectively, between 3 and 29 GeV.

There are now sufficient data available to map out, in a rather complete fashion, the distribution of isotopic yields in this mass region. Klapisch, *et al.*[24] have measured the isotopic distribution of Na nuclides produced in GeV proton bombardments of a number of targets. Their isotopic Na distributions show that the yields for all targets peak either on stability or slightly to the neutron-excess side of it, Na^{23}–Na^{25}, and the yields drop off rapidly at both higher and lower mass numbers. Previously measured ratios of the independent yield of Na^{24} to the cumulative yield of Ne^{24}, $Na^{24}(i)/Ne^{24}(c)$, from various targets[25] show that isobaric yields also are at a maximum near stability.

The same argument seems to hold true for neutron-deficient isobars. Subtracting values of $\sigma_{Na^{22}}(i)$ of Klapisch, *et al.*[24] from published values[12] of $\sigma_{Na^{22}}(c)$ gives at least a rough idea of $\sigma_{Mg^{22}}(c)$. For heavy targets, Ir, Au, and U, $\sigma_{Na^{22}}(i) \approx \sigma_{Na^{22}}(c)$ indicating a steep drop-off in yield on the neutron-deficient side of the stability valley. For medium-mass targets, Ag and Mo, and presumably for lighter ones too, $\sigma_{Na^{22}}(i) < \sigma_{Na^{22}}(c)$. These facts show that most fragments are produced close to stability, with yields dropping off quickly whether one looks at isobaric or isotopic distributions. The main effect of increasing target mass on the yield distribution, aside from increasing total yields, is the higher probability of making neutron-excess species. This fact in itself is not unexpected, since the heavier targets also have greater neutron/proton ratios. The fact that the peak positions of the distributions change very little perhaps is suprising.

There have been arguments presented previously[25] that the mechanism by which these fragments are produced cannot be one in which the struck nucleus is shattered so quickly that the small fragment retains only a neutron/proton ratio similar to that of the parent with a greater or lesser amount of excitation energy. Calculations based on this hypothesis predict that from neutron-rich targets, such as Au and U, no neutron-deficient products would be formed. The observed charge distributions, the small but significant yields of neutron-deficient species, and the apparent odd-even effect in the independent Na yields[24] all point to the conclusion that even in very complex reactions involving large intranuclear cascades and high levels of excitation, the difference of a few MeV in the final products is important; phase-space considerations muct play an important role not only in the last few deexcitation steps, but in the initial break up as well.

Ar. The Ar yields measured in this work plus additional data in the same mass region from other workers are shown in Table III. There is little doubt that products in the mass region 36–42 are spallation products when Cu is bombarded with 3- or 29-GeV protons. Between these two energies all measured Ar yields decrease ~15%, which may be considered complementary to the similar precentage increase in the Ne yields. At the higher incident energy there is a greater probability for very complex reactions to occur, and these occur at the expense of those reactions which are less complex.

The isotopic-distribution curves for the Ar isotopes from Cu at 3 and 29 GeV are approximately Gaussian in shape and almost identical at the two energies. The maxima of the curves occur at an N/Z value of 1.12. Attempts at similar isotopic-distribution analyses of the Ar data are not as satisfactory for Ag, Au, and U targets. The shapes of the distributions are not Gaussian, and it is difficult to obtain a precise value for the most probable N/Z value for each target. However, if one ignores the K^{42} data, as was done by Katcoff, Fickel, and Wyttenbach (KFW),[13] the Ag results yield ~1.15 for the most probable value of N/Z in the mass-40 region. The same value was obtained by KFW[13] using a wider mass range.

The yields of the neutron-deficient species Ar^{36} and Ar^{37} are greater from Ag than from either Au or U at both 3 and 29 GeV. One can interpret the mass-yield curves from Ag[13] to indicate that the yields at $A \sim 36$–40 are the tail of the spallation-product distribution, and the agreement, at least at 3 GeV, between the experimental results and the spallation yield calculations, shown in Table I, is also satisfactory. From Au and U the distribution of the Ar yields shows that products in the mass-40 region are not produced by a spallation

TABLE III. Formation cross sections, in mb, of nuclides in the $A=36-42$ mass region as a function of target mass and incident energy.

	Target							
	Cu		Ag		Au-Pb		U	
Product	3 GeV	29 GeV	3 GeV	29 GeV	3 GeV	29 GeV	3 GeV	29 GeV
Ar^{36}	1.4	1.2	0.31	0.47	~0.1	0.28	<0.5	0.20
Ar^{37}	5.4	4.7	1.2	2.3	0.52	1.6	0.40	1.6
Ar^{38}	13.4	11.1	4.4	7.0	4.7	9.4	11.2	15.3
Ar^{39}	7.2	6.4	2.7	4.7	3.5	7.8	7.0	13.0
Ar^{41}	0.87[a]	0.73[a]	0.41[b]	0.63[b]		1.43[c]	1.98[c]	4.3[c]
Ar^{42}	0.17	0.16	0.12	0.21	0.42	0.82	1.2	2.0
K^{42}	2.90[a]	2.83[a]	1.67[b]	0.99[b]	1.82[d]		4.0[d]	
Cl^{39}					0.8[d]			
Cl^{38}					1.33[d]			

[a]Ref. 23.
[b]Ref. 13.
[c]R. Stoenner, private communication.
[d]G. Friedlander and L. Yaffe, Phys. Rev. 117, 578 (1960).

mechanism. As was stated above, the yields of neutron-deficient nuclides from Au and U are depressed relative to Ag, and the observed increase in total chain yields (Ar^{38}) arises from neutron-excess species. The difference between Au and U is most significant on the neutron-excess wing of the isotopic distribution. For example, at 29 GeV, whereas the total yield at $A=38$ is 9.4 mb from Au and 15.3 mb from U, which is an increase of less than a factor of 2, the yields of neutron-excess Ar^{41} and Ar^{42} from U are factors of 2.5 to 3 times those from Au. The isotopic distributions and general shapes of the mass-yield curves show that both Ne and Ar yields from heavy elements are neither spallation residues nor "normal" fission products, but result from the same processes which lead to even higher yields of lighter fragments.

The possibility that the evaporation mechanism encompasses the yield of fragments as heavy as Ar isotopes cannot be ruled out. Dostrovsky, *et al.*[26] have shown that the ratio of fragment yields, as heavy as Na, from various heavy nuclei are in agreement with calculations based on the statistical theory of evaporation. More recently, Crespo, Cummings, and Alexander,[27] following a suggestion of Swiatecki,[28] have proposed that in a unified liquid-drop theory of fission and evaporation there are two saddle points. One saddle point is at symmetric mass division (fission) and the other at very asymmetric mass splits (evaporation). The potential peak between the two saddle points would lead to a minimum in the mass-yield curve, as is observed with U (Fig. 5), and perhaps also in Au (Fig. 4).

Kr *and* Xe. Kr isotopes are produced by spallation from Ag at both 3 and 29 GeV. The pattern of Kr yields from Ag is very similar to that of the Ar yields from Cu, which is not suprising since ΔA, the mass difference between target and product, is the same in both cases. The Kr data have also been used by KFW,[13] and from their analysis one can see that the slopes of the mass-yield curves at 3 and 29 GeV are such that products with mass number ≥ 60 are formed in higher yield at 3 GeV. Below $A=60$ the reverse is true, and the ratio of yields at 29 GeV compared with 3 GeV increases steadily with decreasing mass. KFW obtained a most probable N/Z of 1.19 in the mass region 76–86 which corresponds to Kr^{80}. Thus the peaks of the isobaric distributions lie slightly to the neutron-deficient side of stability, but the distributions are wide enough to have some contribution from slightly neutron-excess nuclides such as Kr^{84} and Kr^{85}. No $Kr^{86}(N/Z=1.39)$ was detected from $Ag(N/Z=1.30)$ at either energy.

The neutron-excess Kr isotopes 84, 85, and 86 are produced in higher yield from Au than from Ag targets, and the spallation calculations in Table I underestimate the observed cross sections. Both of these facts lead to the conclusion that the fission of Au leads to non-negligible yields of Kr isotopes, especially of those species which are rich in neutrons. This seems to be true especially at 3 GeV. At the higher energy, the yields of the neutron-rich products decrease slightly, although total yields (Kr^{83}) rise by ~10–15%. The increase in the calculated spallation cross sections and the observed slight decrease (10–20%) in the measured fission cross section between 3 and 29 GeV[16] indicate that as the energy is raised above 3 GeV, spallation plays a larger role in producing nuclides ~100 mass units away from the Au target. The same is not true of the Xe yields from Au. Here, essentially no neutron-excess products are formed, and the spallation calculations agree with the measured yields at both energies.

For U products in the 130 mass region, charge-

dispersion curves of Friedlander, *et al.*[14,29] and Chu, *et al.*[30] exhibit two peaks in the yield distribution. One peak, composed mainly of neutron-excess species, is attributed to low-energy fission processes. The other peak contains mainly neutron-deficient species and its height, relative to the neutron-excess peak, increases with increasing bombardment energy. From Table II it can be seen that the independent yields from U of I^{126}, Xe^{129}, and Xe^{131}, agree quite well with the results of Friedlander.[14] These three nuclides all fall near the maximum of the neutron-deficient peak as defined in that work, and thus confirm, by a completely independent experimental technique, the magnitude of that peak.

Neutron-deficient nuclides are produced from U + GeV protons by at least two processes. Crespo, Cumming, and Poskanzer[31] have shown that high-energy fission contributes to the observed yield. In addition, the recoil measurements of Brandt,[32] Crespo, Cumming, and Poskanzer,[31] and Ravn and Hagebø[33] all show that at least in the mass-115–130 region, spallation processes are necessary to account for very neutron-deficient species with low recoil velocities. The calculated curve in Fig. 5 shows that there is a small but real spallation contribution under the fission peak.

To summarize, fragment emission, whether from evaporation or other mechanisms, accounts for observed yields up to $A \sim 20$–30 for Cu and Ag targets, and spallation accounts for yields between this mass region and that of the target. The yield of light fragments from Au extends to $A \sim 40$, and between $A = 40$–140 the observed yields seem to be mainly spallation products, with a small contribution from fission. Fragments emission from U also extends to $A \sim 40$, but the major contribution to yields in the 40–140 mass region is now chiefly fission with spallation prosesses contributing only near the upper end of the region.

ACKNOWLEDGMENT

We wish to thank the operating staff of the AGS for their assistance with the irradiations, Miss E. Norton and Miss B. Nine for performing the chemical analyses and R. W. Schlott for his skilled glass-blowing assistance.

---

†Research performed under the auspices of the U. S. Atomic Energy Commission, partially under Contract No. AT-(30)-3629.

*Present address: Max-Planck-Institut für Kernphysik, Heidelberg, Germany.

[1]R. Klapisch, Ann. Rev. Nucl. Sci. 19, 33 (1969).

[2]R. Bernas, E. Gradsztajn, R. Klapisch, F. Yiou, and N. Long Den, Nucl. Instr. and Methods 37, 141 (1965).

[3]T. Kirsten, "Determination of Radiogenic Argon" in Potassium-Argon Dating, edited by O. A. Schaeffer and J. Zähringer (Springer Publishers, New York, 1966), p. 7.

[4]J. B. Cumming, J. Hudis, A. M. Poskanzer, and S. Kaufman, Phys. Rev. 128, 2392 (1962).

[5]J. B. Cumming, G. Friedlander, J. Hudis, and A. M. Poskanzer, Phys. Rev. 127, 950 (1962).

[6]R. W. Stoenner, O. A. Schaeffer, and S. Katcoff, Science 148, 1325 (1965).

[7]J. B. Cumming, National Academy of Sciences–National Research Council, Nuclear Science Series No. NAS-NS-3107, 1962 (unpublished), p. 25.

[8]National Academy of Sciences Committee on Nuclear Science, Radiochemistry Monographs No. 3055 (Clearing House for Federal Scientific and Technical Information, Springfield, Virginia, 1962).

[9]We wish to thank S. Katcoff for these targets.

[10]G. Friedlander, J. Hudis, and R. Wolfgang, Phys. Rev. 99, 263 (1955).

[11]V. P. Crespo, J. M. Alexander, and E. K. Hyde, Phys. Rev. 131, 1765 (1963).

[12]J. Hudis and S. Tanaka, Phys. Rev. 171, 1297 (1968).

[13]S. Katcoff, H. R. Fickel, and A. Wyttenbach, Phys. Rev. 166, 1147 (1968).

[14]G. Friedlander, in Proceedings of the Symposium on the Physics and Chemistry of Fission, Salzburg, Austria, 1965 (IAEA, Vienna, Austria, 1965), Vol. II, p. 265.

[15]The point at $A = 7$ is from R. Klapisch, Ph.D. thesis, Institute of Nuclear Physics, Orsay, 1966 (unpublished).

[16]J. Hudis and S. Katcoff, Phys. Rev. 180, 1122 (1969).

[17]G. Rudstam, Z. Naturforsch. 21a, 1027 (1966).

[18]U. Schwarz and H. Oeschger, Z. Naturforsch. 22a, 972 (1967).

[19]N. Metropolis, R. Bivens, M. Storm, A. Turkevich, J. M. Miller, and G. Friedlander, Phys. Rev. 110, 185, 204 (1958).

[20]K. Chen, Z. Fraenkel, G. Friedlander, J. R. Grover, J. M. Miller, and Y. Shimamoto, Phys. Rev. 166, 949 (1968).

[21]I. Dostrovsky, P. Rabinowitz, and M. Storm, Phys. Rev. 111, 1659 (1958).

[22]I. Dostrovsky, Z. Fraenkel, and G. Friedlander, Phys. Rev. 116, 683 (1959).

[23]J. Hudis, I. Dostrovsky, G. Friedlander, J. R. Grover, N. T. Porile, L. P. Remsberg, R. W. Stoenner, and S. Tanaka, Phys. Rev. 129, 434 (1963).

[24]R. Klapisch, C. Philippe, J. Suchorzewska, C. Detraz, and R. Bernas, Phys. Rev. Letters 20, 740 (1968) and C. Philippe-Thibault, private communication.

[25]J. Hudis, Phys. Rev. 171, 1301 (1968).

[26]I. Dostrovsky, R. Davis, Jr., A. M. Poskanzer, and P. L. Reeder, Phys. Rev. 139, B1513 (1965).

[27]V. P. Crespo, J. B. Cumming, and J. M. Alexander, to be published.

[28]W. J. Swiatecki, private communication to authors of Ref. 27.

[29]G. Friedlander, L. Friedman, B. Gordon, and L. Yaffe, Phys. Rev. 129, 1809 (1963).

[30]Y. Y. Chu, E-M. Franz, G. Friedlander, and P. Kar-

ol, to be published.
[31]V. P. Crespo, J. B. Cumming, and A. M. Poskanzer, Phys. Rev. 174, 1455 (1968).
[32]R. Brandt, in Proceedings of the Symposium of the Physics and Chemistry of Fission, Salzburg, Austria, 1965 (IAEA, Vienna, Austria, 1965), Vol. II, p. 329.
[33]H. Ravn and E. Hagebø, J. Inorg. Nucl. Chem. 31, 2649 (1969).

PHYSICAL REVIEW C VOLUME 1, NUMBER 6 JUNE 1970

Energy Levels of Lu^{174}

H. D. Jones* and R. K. Sheline
The Florida State University, Tallahassee, Florida† 32306
(Received 27 October, 1969)

Thirty-two levels in Lu^{174} have been observed up to an excitation energy of 1628 keV utilizing 12-MeV deuterons and the reaction $Lu^{175}(d,t)Lu^{174}$. The ground-state Q value was determined to be -1400 ± 15 keV. The spectrum has been interpreted in terms of the coupling of the [404↓] Nilsson proton orbital with the neutron orbitals prominent in the (d,t) spectrum of Yb^{173}. This interpretation has resulted in the determination of relative energies due to the residual neutron-proton interaction for seven different configurations. The observed singlet-triplet splitting energies for the [512↑], [521↓], and [521↑] neutron orbitals coupled to the [404↓] proton orbital were measured to be −110, +80, and −90 keV, respectively. Theoretical calculations of these energies made for a zero-range spin-dependent central potential gave values of −106, +71, and −77 keV, respectively. The remarkable agreement indicates that the spin-spin interaction can account for most, if not all, of the singlet-triplet splitting energy.

INTRODUCTION

One of the more complex aspects of nuclear physics is the study of odd-odd deformed nuclei. These nuclei can be approximately described as consisting of an inert tightly bound core plus an extra proton and an extra neutron which are relatively free compared to the particles in the core. The interaction between the odd particles has a strong influence on the energies of low-lying states. However, the rotational motion of the deformed system still dominates the low-energy spectrum, especially for well-deformed nuclei. Thus the low-energy spectra of these nuclei consist of intrinsic states with superimposed rotational levels whose relative energies are well described by the rotational formula

$$E = \frac{\hbar^2}{2\mathcal{I}} I(I+1), \tag{1}$$

where $\mathcal{I}$ is the moment of inertia and I is the total angular momentum of the nucleus. The reaction cross sections of these rotational levels follow a definite pattern or "fingerprint" which is characteristic of the intrinsic state on which the rotational band is superimposed. The value of I for the band head (usually the member of the band with the lowest energy) is characteristic of the intrinsic state on which the rotational band is built. The approximate energies of intrinsic states can be determined by using the Nilsson model[1] to describe the single-particle states in the deformed nucleus. This model also furnishes the wave functions which are used to calculate the reaction cross sections. Even better estimates of the approximate energies can be made if the spectra of neighboring odd-A nuclei have been interpreted in terms of the Nilsson model. In order to improve the cross sections we have utilized a modified Nilsson model[2] which uses a more realistic Woods-Saxon potential and includes certain coupling terms which were ignored in the original Nilsson model.

The intrinsic-energy estimates, along with the energy systematics described by Eq. (1) and the characteristic intensity pattern or "fingerprint," provide a means of interpreting the spectra of deformed nuclei. Second-order mixing effects sometimes distort the intensity pattern, but these effects can usually be predicted accurately within the framework of the rotational model.[3]

Once interpretation of the energy levels has been made, the energy shifts due to the neutron-proton residual interaction can be extracted from the observed energies and compared to theoretical calculations for various choices for the form of the two-body potential. The purpose of this paper is therefore not only a detailed spectroscopic study of the levels of Lu^{174}, but also to provide experimental values of residual interaction energies in Lu^{174} and to compare these to calculations for a simple type of neutron-proton interaction.

Since excited neutron states have been studied extensively in odd-A nuclei in the rare-earth region, the most promising approach is to study states in Lu^{174} in which only the state of the odd